PNAS RESEARCH ARTICLE | NEUROSCIENCE OPEN ACCESS

Mice lacking *Astn2* have ASD-like behaviors and altered cerebellar circuit properties

Michalina Hanzel[a], Kayla Fernando[b], Susan E. Maloney[c], Zachi Horn[a,d], Shiaoching Gong[e], Kärt Mätlik[a], Jiajia Zhao[a], H. Amalia Pasolli[f], Søren Heissel[g], Joseph D. Dougherty[c,h], Court Hull[b], and Mary E. Hatten[a,1]

Affiliations are included on p. 11.

Contributed by Mary E. Hatten; received March 27, 2024; accepted July 5, 2024; reviewed by Mustafa Sahin, Roy Sillitoe, and Samuel S. Wang

Astrotactin 2 (ASTN2) is a transmembrane neuronal protein highly expressed in the cerebellum that functions in receptor trafficking and modulates cerebellar Purkinje cell (PC) synaptic activity. Individuals with *ASTN2* mutations exhibit neurodevelopmental disorders, including autism spectrum disorder (ASD), attention-deficit/hyperactivity disorder (ADHD), learning difficulties, and language delay. To provide a genetic model for the role of the cerebellum in ASD-related behaviors and study the role of ASTN2 in cerebellar circuit function, we generated global and PC-specific conditional *Astn2* knockout (KO and cKO, respectively) mouse lines. *Astn2* KO mice exhibit strong ASD-related behavioral phenotypes, including a marked decrease in separation-induced pup ultrasonic vocalization calls, hyperactivity, repetitive behaviors, altered behavior in the three-chamber test, and impaired cerebellar-dependent eyeblink conditioning. Hyperactivity and repetitive behaviors are also prominent in *Astn2* cKO animals, but they do not show altered behavior in the three-chamber test. By Golgi staining, *Astn2* KO PCs have region-specific changes in dendritic spine density and filopodia numbers. Proteomic analysis of *Astn2* KO cerebellum reveals a marked upregulation of ASTN2 family member, ASTN1, a neuron–glial adhesion protein. Immunohistochemistry and electron microscopy demonstrate a significant increase in Bergmann glia volume in the molecular layer of *Astn2* KO animals. Electrophysiological experiments indicate a reduced frequency of spontaneous excitatory postsynaptic currents (EPSCs), as well as increased amplitudes of both spontaneous EPSCs and inhibitory postsynaptic currents in the *Astn2* KO animals, suggesting that pre- and postsynaptic components of synaptic transmission are altered. Thus, ASTN2 regulates ASD-like behaviors and cerebellar circuit properties.

autism spectrum disorder | cerebellum | Purkinje cell | ASTN2 | neurodevelopmental disorder

Significance

Autism spectrum disorder (ASD) is a complex neurological disorder characterized by social deficits and repetitive behaviors. Individuals with mutations in the Astrotactin 2 (*Astn2*) gene display a range of developmental disorders, including ASD. Here, we examine the role of *Astn2*, a predominantly cerebellar gene, in cerebellar function and behaviors associated with ASD. Knocking out *Astn2* in mice results in ASD-like behaviors as well as altered cerebellar structure and function. *Astn2* knockout (KO) mice have region-specific changes in dendritic spine density and filopodia numbers as well as a significant increase in Bergmann glia volume. Electrophysiological experiments indicate that pre- and postsynaptic components of synaptic transmission are altered. We demonstrate that *Astn2* is important for cerebellar function and mouse behavior.

Astrotactin 2 (ASTN2) is a vertebrate-specific neuronal glycoprotein with important roles in trafficking proteins including synaptic receptors (1), as well as the neuron–glial adhesion protein ASTN1 that functions in glial-guided neuronal migration (2, 3). ASTN2 expression levels are highest in cerebellar Purkinje cells (PCs) and granule neurons, with lower levels of expression in the neocortex, olfactory bulb, and dentate gyrus of the hippocampus (1, 3). Copy number variations (CNVs) in *ASTN2* have been identified as a significant risk factor for Autism spectrum disorder (ASD) in many studies (4, 5), and *ASTN2* is listed as a gene implicated in ASD susceptibility by the SFARI initiative of the Simons Foundation. *Astn2* is also highly coexpressed with other autism-related genes, especially in the cerebellum (6). Additionally, we recently reported a family with a paternally inherited intragenic *ASTN2* duplication, which results in *ASTN2* haploinsufficiency. The family manifests a range of neurodevelopmental disorders, including ASD, learning difficulties, and speech and language delay (1). The high levels of ASTN2 expression in the mouse cerebellum, starting at embryonic stages and high at all postnatal stages, suggest that *ASTN2* mutations such as those found in patients with *ASTN2* CNVs could lead to altered cerebellar function. Furthermore, our cellular and molecular studies on mouse cerebellum show that ASTN2 binds to and regulates the trafficking of multiple synaptic proteins, many of which are implicated in ASD, and modulates cerebellar PC synaptic activity (1). We therefore generated *Astn2* global and conditional knockout (KO) mouse lines to examine whether ASTN2 loss affects ASD-associated behaviors and cerebellar circuit properties.

Although the cerebellum has long been considered to be a purely motor structure, recent studies reveal that it also has critical nonmotor functions, including language (7), social cognition (8), and emotional processing (9). Cerebellar activation is observed in humans during social cognition tasks (10), and stimulation of the mouse cerebellum modulates dopamine release in the medial prefrontal cortex of wild-type (WT) animals, but not in several

Preprint servers: Manuscript submitted to Biorxiv as a preprint.

Reviewers: M.S., Boston Children's Hospital; R.S., Baylor College of Medicine; and S.S.W., Princeton University.

The authors declare no competing interest.

[1]To whom correspondence may be addressed. Email: hatten@rockefeller.edu.

This article contains supporting information online at https://www.pnas.org/lookup/suppl/doi:10.1073/pnas.2405901121/-/DCSupplemental.

Published August 16, 2024.

mouse models of ASD (11). Recent studies demonstrate a direct, monosynaptic pathway from the cerebellum to the ventral tegmental area that controls social behaviors (12) and show that the cerebellar-prefrontal cortex circuits mediate cerebellum-regulated social and repetitive/inflexible behaviors (13). Moreover, a loss of cerebellar PCs is one of the most consistent structural findings in postmortem studies of patients with ASD (14) and cerebellar injury at birth results in an approximately 40-fold increase in ASD by age two (15). In addition, specific targeting of cerebellar PCs in mouse models of ASD-associated genes leads to impaired cerebellar learning (16) and social behaviors (17–19). Thus, cerebellar dysfunction is strongly implicated in ASD.

In the present study, we generated global and conditional loss of function *Astn2* mouse lines and analyzed their ASD-related behaviors and cerebellar circuit properties. We found that mice lacking *Astn2* have deficits in social behaviors and in the number and properties of ultrasonic vocalization (USV) calls, as well as an increase in repetitive behaviors and hyperactivity, all behavioral changes that are characteristic of ASD (20). Importantly, the hyperactivity and repetitive behavior changes were also found in a mouse line with a conditional loss of *Astn2* specific to PCs, suggesting a role for the cerebellum in these behaviors. Consistent with this finding, the ASD-like behaviors were accompanied by changes in the structure of PC dendritic spines in the posterior vermis and Crus1 of *Astn2* KO animals, areas associated with repetitive behaviors and social behaviors, respectively (13). Molecular studies revealed an upregulation of the neuron–glial adhesion protein ASTN1 with concomitant changes in the volume of Bergmann glial fibers in the molecular layer. Finally, we also observed changes in cerebellar circuit properties evidenced by changes in spontaneous excitatory postsynaptic current (EPSCs) and inhibitory postsynaptic current (IPSCs). These studies suggest that ASTN2 functions in ASD-like behaviors and cerebellar circuit properties, and show, in agreement with other studies on cerebellar circuits in ASD (18), that even subtle changes in cerebellar anatomy and physiology can lead to significant behavioral changes.

Results

Generation of *Astn2* Global and Conditional KO Lines. The *Astn2* KO mouse line was generated using CRISPR-Cas9 technology by targeting the first exon and the promoter region of the *Astn2* gene (see the *Materials and Methods* section for details). The loss of ASTN2 protein expression was confirmed using western blot analysis (*SI Appendix*, Fig. S1) and the proteomic analysis of whole cerebellar tissue (Fig. 5). *Astn2* KO mice did not show reduced survival or fertility and their weights were comparable across genotypes at P22. The gross morphology of the cerebellum, including the size and weight, foliation pattern, cell densities, and layer formation, was normal (*SI Appendix*, Fig. S2). We did not observe any abnormalities in cerebellar neurogenesis, granule cell proliferation, or glial-guided neuronal migration (*SI Appendix*, Fig. S3). Next, we generated a conditional *Astn2* KO mouse line by inserting two loxP sites flanking exon 1 and the promoter region of the *Astn2* gene using a similar approach as with the global KO mouse (*Materials and Methods*). The $Astn2^{flox/flox}$ line was then crossed with the *Pcp2-Cre* line (Gensat) to generate a PC-specific conditional KO line (*Astn2* cKO, *SI Appendix*, Fig. S1). *Pcp2-cre* starts being expressed at around postnatal day 7. *Astn2* cKO mice did not show reduced survival or fertility, their weights were comparable across genotypes at P22, and no gross abnormalities were observed.

***Astn2* KO Pups Produce Fewer and Less Complex USVs in a Maternal Separation Assay.** Individuals with *ASTN2* CNVs have language deficits (1), and many mouse models of ASD show deficits in USVs in social communication (21–23). To understand the influence of *Astn2* loss of function on early social communication, we measured pup isolation calls induced by maternal isolation (Fig. 1*A*). USVs were recorded after pup isolation at postnatal days (P)5–P14. Loss of *Astn2* expression robustly influenced USV production (Fig. 1*B*). Specifically, *Astn2* KO mice exhibited significantly fewer USVs during the 5-min recording session across P6–P10 (Fig. 1*C* and *SI Appendix*, Table S1). In addition, heterozygous mutants (Het) also showed a significant reduction in call number compared to wild types on P6–P8, demonstrating an intermediate phenotype. This phenotype did not interact with sex (*SI Appendix*, Table S1). We next examined the temporal and spectral call features to determine whether respiratory tract alterations contribute to call variation and whether call complexity is altered following the loss of *Astn2*. Complementary to the number of individual calls, the *Astn2* KO mice also produced fewer bouts of calls, defined as a sequence of calls separated by pauses <0.5 s, compared to Het and WT littermates on days P6–P10. Again, Hets showed an intermediate phenotype with reduced bouts only on day 8 (Fig. 1*D*). In addition, *Astn2* KO mice exhibited longer pauses between calls within a bout compared to WT & Het littermates overall, with a particularly robust decrease at P10 (*SI Appendix*, Table S1). We found that overall *Astn2* KO mice produced shorter individual calls compared to both heterozygous $Astn2^{+/-}$ and WT littermates (Fig. 1*E*). We also examined spectral features of the calls. We observed a significant narrowing of frequency pitch range in all the calls produced by *Astn2* KO mice at ages P6–P10 compared to those produced by their heterozygous *Astn2* and WT littermates (Fig. 1*F*). No differences were observed for the average frequency pitch or the peak amplitude of the sound pressure level (loudness) of all calls produced by the mice (*SI Appendix*, Table S1). Next, we separated the calls into those that contain a frequency pitch jump, known as dynamic calls, and those that do not contain a pitch jump, known as flat calls. We observed a significant decrease in the fraction of dynamic calls produced by *Astn2* KO mice, which was particularly robust P6–P10, compared to heterozygous *Astn2* and WT littermates (Fig. 1*G*). The average pitch and pitch range of dynamic calls were not largely different between groups (*SI Appendix*, Table S1). While the flat calls produced by *Astn2* KO did not differ in their average pitch, they were significantly narrowed in their pitch range compared to heterozygous *Astn2* and WT littermates, particularly at P7–P10 (Fig. 1*H*). In conclusion, a loss of *Astn2* in the mouse results in a robust decrease in USV production, particularly during the peak age range for this behavior (P6–P10), and significantly influences the spectral pitch range of the produced calls.

***Astn2* KO Animals Show Defects in Social Behaviors in the Three-Chamber Test.** Individuals with ASD show abnormalities in social behavior. To understand the influence of *Astn2* on social behaviors, we evaluated social behaviors in adult mice (8 to 12 wk of age) in the three-chamber sociability and social novelty tests. In this paradigm, the test mouse was placed in the middle chamber of the three-chamber apparatus with two empty wire baskets in the other two chambers (Fig. 2*A*). The test consisted of three phases starting with an initial 10-min habituation period to the empty baskets. In the second phase, a social stimulus (a novel mouse) was placed in one of the baskets and a nonsocial stimulus, such as a Lego block, was placed in the other basket. The time that the test mouse spent investigating the two stimuli was measured. A typical WT mouse prefers to spend time with a social stimulus. In the third phase, the familiar mouse was left in their basket and the nonsocial stimulus was exchanged for a novel mouse. In this case, a typical WT mouse prefers to spend time with a novel mouse instead of the familiar mouse. In our experiments, *Astn2* KO mice showed an overall

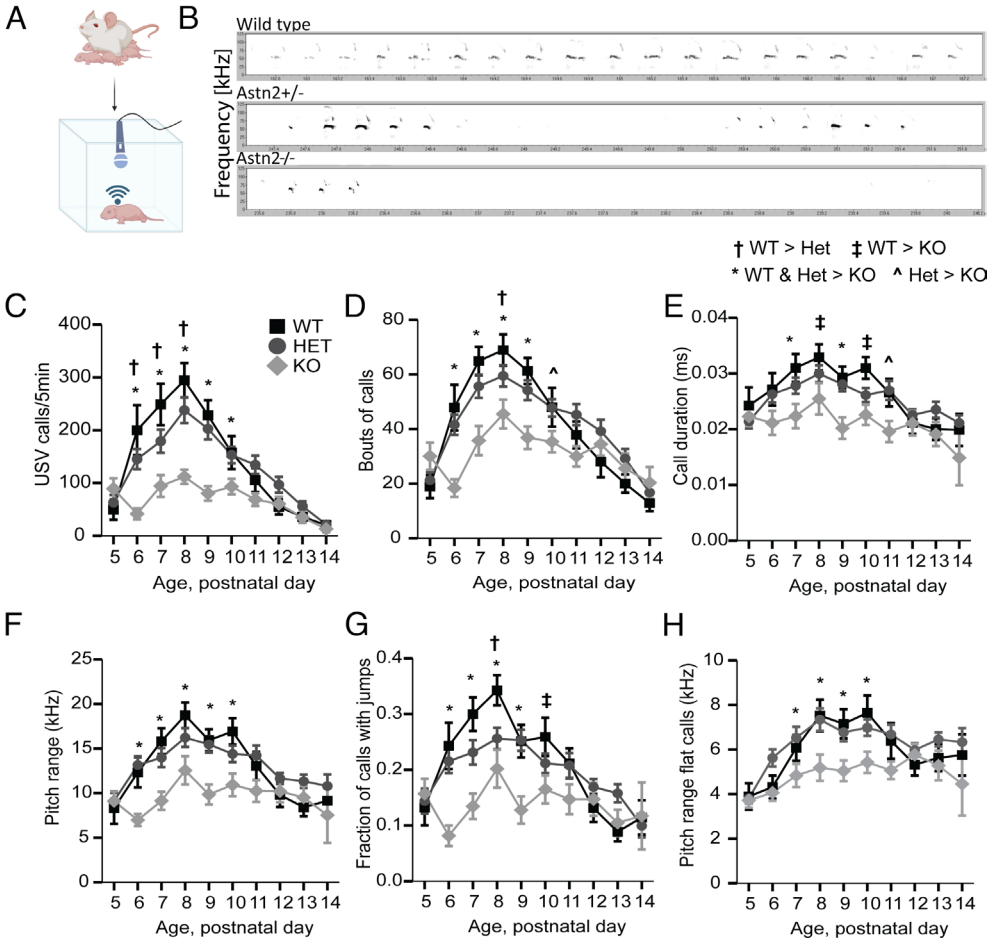

Fig. 1. Loss of *Astn2* results in fewer and less dynamic USVs in the mouse pups. (*A*) Pups were isolated from their mothers at postnatal days (P)5–P14 and placed in a soundproof chamber fitted with an ultrasonic microphone. USVs were recorded for 5 min. (*B*) Sample spectrograms illustrating the differences in USVs from P7 WT (n = 20), heterozygous (HET) (n = 52), and *Astn2* KO (n = 24) animals (frequency in kHz as a function of time). Loss of ASTN2 expression robustly influenced USV production and dynamics on a number of measures at P6–P10: (*C*) Number of USV calls during the 5-min recording session was reduced in *Astn2* KOs. Heterozygous animals showed a significant reduction at P6–P8. (*D*) Bouts of calls were reduced in *Astn2* KOs. (*E*) Call duration was reduced in *Astn2* KOs. (*F*) Pitch range of all USV calls was reduced in *Astn2* KOs. (*G*) Fraction of calls that are dynamic (contain a pitch jump) was reduced in *Astn2* KOs. Heterozygous animals show a reduction in dynamic calls at P8. (*H*) Range of frequency pitch for flat calls was reduced in *Astn2* KOs at P7–P10. Data are presented as beans ±SEM. Symbols represent statistically significant results between the genotypes as described in the legend within the figure. Statistical analysis can be found in *SI Appendix*, Table S1.

preference for a social, rather than a nonsocial stimulus, similar to their WT littermates. However, they spent significantly less total time investigating the social stimulus compared to WT mice (around 25% decrease in time spent) (Fig. 2*B* and *SI Appendix*, Table S2). Additionally, while WT littermates spent significantly longer investigating the novel mouse (around 40% more time), *Astn2* KOs did not show a preference for the novel mouse and spent similar amount of time investigating the novel and the familiar counterparts (Fig. 2*C* and *SI Appendix*, Table S2). Therefore, *Astn2* KO mice exhibit abnormal social behavior.

***Astn2* KO Animals Are Hyperactive and Show Repetitive Behaviors and Reduced Anxiety in an Open-Field Assay.** One of the most prominent features of individuals with ASD is repetitive behavior. Some patients also show hyperactivity and/or an increase in anxiety. We used the open-field experimental assay to measure these behaviors in *Astn2* KO mice. Eight- to twelve-week-old animals were placed in an open arena for 1 h and allowed to explore freely (Fig. 2*D*). We found that *Astn2* KO mice traveled a significantly longer distance in the arena, around 30% more, compared to their WT and heterozygous littermates (Fig. 2*E* and *SI Appendix*, Table S3). Additionally, *Astn2* KO mice displayed a number of behaviors that are suggestive of repetitive behaviors, including around 20% increase in rearing (standing vertically on their hind paws) (Fig. 2*F* and *SI Appendix*, Table S3) and an increase by 40% in the number of revolutions (circling in place) compared to WT mice (Fig. 2*G* and *SI Appendix*, Table S3). Anxiety-like phenotypes can also be measured in the open-field paradigm. Typically, mice prefer to spend more time toward the periphery of the arena and avoid the center. Spending a higher proportion of time in the periphery is indicative of heightened anxiety-like avoidance behaviors and spending more time in the center is indicative of lowered anxiety. *Astn2* KO animals spent significantly less time in the periphery of the arena compared to WT littermates (Fig. 2*H* and *SI Appendix*, Table S3) suggesting lowered anxiety. An additional measure of anxiety-like behavior involves using the light/dark box where half of the arena is covered by a dark box (Fig. 2*I*). Mice that prefer to spend more time in the dark versus the light compartment or take longer to enter the light area are exhibiting more avoidance behavior. *Astn2* KO mice did not show a preference for the dark compartment (Fig. 2*J* and *SI Appendix*, Table S3) but had significantly lower latency to enter the light compartment compared to control littermates (Fig. 2*K* and *SI Appendix*, Table S3). Therefore, *Astn2* KO mice exhibit hyperactivity and repetitive behaviors and display lowered anxiety phenotypes.

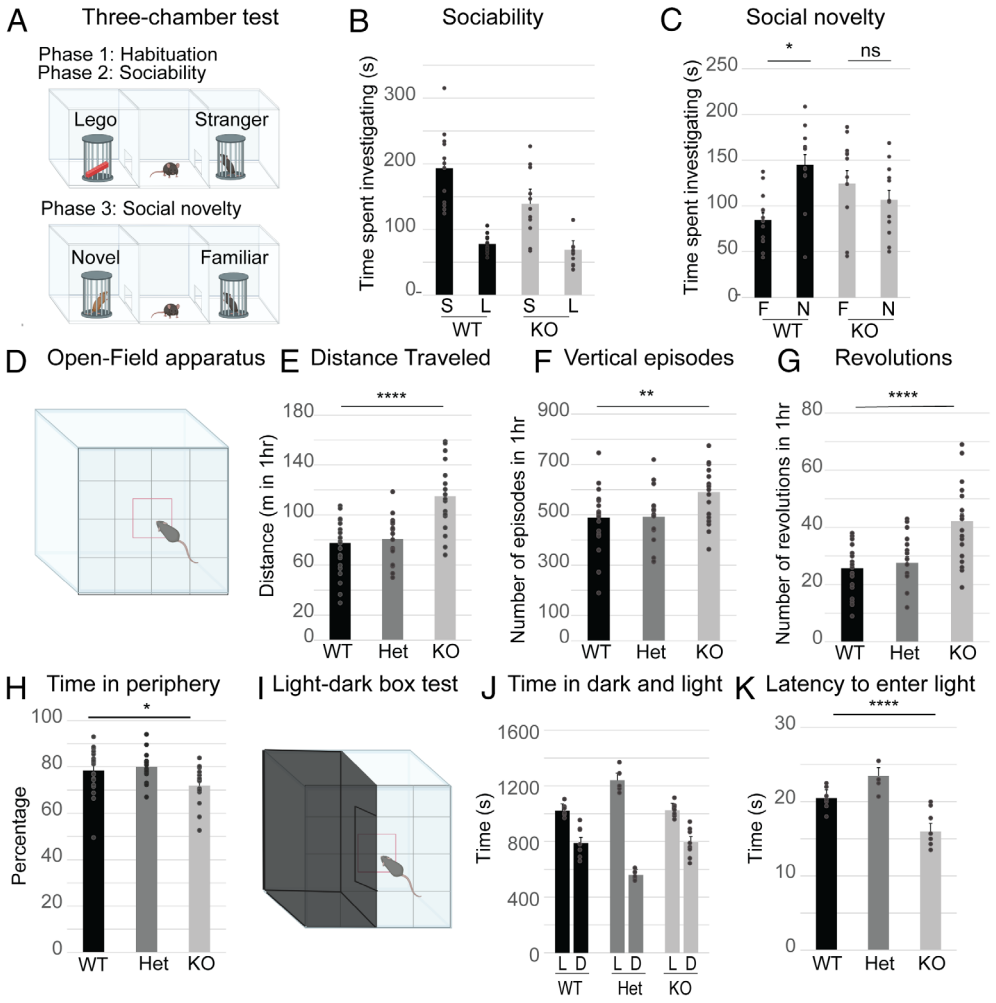

Fig. 2. *Astn2* KO mice show ASD- like behaviors. (*A–C*) Social behavior is altered in the *Astn2* KO mice. (*A*) The three-chamber social test was performed on 8 to 12-week-old animals (n = 12 WT, 11 KO). The test consisted of three phases, starting with a 10-min habituation to the empty cages, followed by two 10-min testing phases. In phase 2, to test sociability, mice were exposed to a nonsocial (Lego block) and a social stimulus (stranger mouse). In phase 3, to test social novelty preference, the nonsocial stimulus was replaced by a novel mouse. The familiar mouse from phase 2 was left in their cage. The time spent interacting with the stimuli was manually scored by the investigator. (*B*) In the first phase of the experiment, WT mice show a strong preference for the social stimulus (S) rather than the Lego block (L) ($P < 0.0001$). *Astn2* KO animals also show a preference for the social stimulus ($P = 0.001$), however, the absolute time they spend interacting with the social stimulus is significantly reduced as compared to the WT ($P = 0.027$). (*C*) In the third phase of the experiment, WT animals interact with the novel animals (N) significantly longer than with the familiar animals (F) ($P = 0.0003$). In contrast, the *Astn2* KO animals do not show a preference for the novel animal and spend as much time with the familiar animal as with the novel animal ($P = 0.35$). Data are analyzed with two-tailed unpaired Student's *t* test and presented as the mean + SEM. (*D–K*) *Astn2* KO mice show hyperactivity and repetitive behaviors, but not anxiety, in the open-field test. (*D*) 8- to 12-week-old WT (n = 29), heterozygous (n = 17), and *Astn2* KO (n = 23) animals were placed in an open-field arena for 1 h and allowed to explore freely. The center of the arena was assigned in the software. (*E*) The total distance traveled was increased significantly in the KO animals ($P < 0.0001$). (*F*) The number of vertical episodes (rearing) was significantly increased in the *Astn2* KOs as compared to WTs and Hets ($P = 0.005$). (*G*) The number of revolutions (circling) was significantly increased in the *Astn2* KOs ($P < 0.0001$). (*H*) Time spent in the center versus the periphery of the arena was measured. *Astn2* KOs spend less time in the periphery of the arena ($P = 0.026$). (*I*) A subset of animals (n = 7 WT, 5 Het, and 8 KO) were tested in a light/dark open-field paradigm where a black box covers half of the arena. (*J*) All genotypes spent significantly more time in the light part of the arena (L) versus the dark part (D), and there were no differences in the amount to time spent in the light (L) versus the dark (D) between WT and KO animals ($P = 0.9$). Het animals spent significantly more time in the light compared to WT and KO animals ($P < 0.0001$). (*K*) The latency to enter the light compartment significantly decreased in the *Astn2* KO ($P < 0.0001$). Data are presented as the mean + SEM. Data are analyzed with one-way ANOVA with Tukey Kramer post hoc test, $*P < 0.05$, $**P < 0.01$, $***P < 0.001$, and $****P < 0.0001$, ns = not significant.

***Astn2* KO Animals Show Abnormal Cerebellar-Dependent Associative Learning.** Individuals with ASD often show abnormal responses to eyeblink conditioning, an associative learning paradigm in which cerebellar circuitry plays a central role (24–27). To assess cerebellar-dependent associative learning, we trained adult (8 to 15 wk old) *Astn2* KO mice and age-matched, WT littermate controls on a delay eyeblink conditioning task (28). Mice were head-fixed on a freely moving cylindrical treadmill (Fig. 3*A*) and conditioned with a 250-ms light stimulus [conditioned stimulus (CS), blue light] and a coterminating, 30-ms corneal air puff [unconditioned stimulus (US), 30 PSI] (Fig. 3 *A* and *B*). Across trials, conditioned responses (CRs) developed as a predictive eyelid closure preceding the US (Fig. 3*B*). On average, we observed a trend toward reduced learning in *Astn2* KO animals relative to controls, with a decrease in CR probability (Fig. 3 *C*, *Top*) and amplitude (Fig. 3 *C*, *Middle*) at later learning timepoints (*SI Appendix*, Table S4, CR_{prob} $P = 0.14$, CR_{amp} $P = 0.22$, two-tailed unpaired Student's *t* test). Notably, however, these averages obscure the variability across individual animals. While all WT animals exhibited learning, five of nine *Astn2* KO animals exhibited little or no learning (Fig. 3 *C* and *D*, *Bottom*). In addition, the *Astn2* KO animals that did learn exhibited altered eyeblink kinematics, displaying more average peaks in their conditioned responses (Fig. 3*D* and *SI Appendix*, Table S4, $P = 0.10$, two-tailed unpaired Student's *t* test; 5 KO mice classified as nonlearners). The behavioral variability across KO animals likely suggests differential genetic compensation in KOs. Overall, these data are consistent with individuals that have ASD, who often produce abnormal conditioned responses after delay

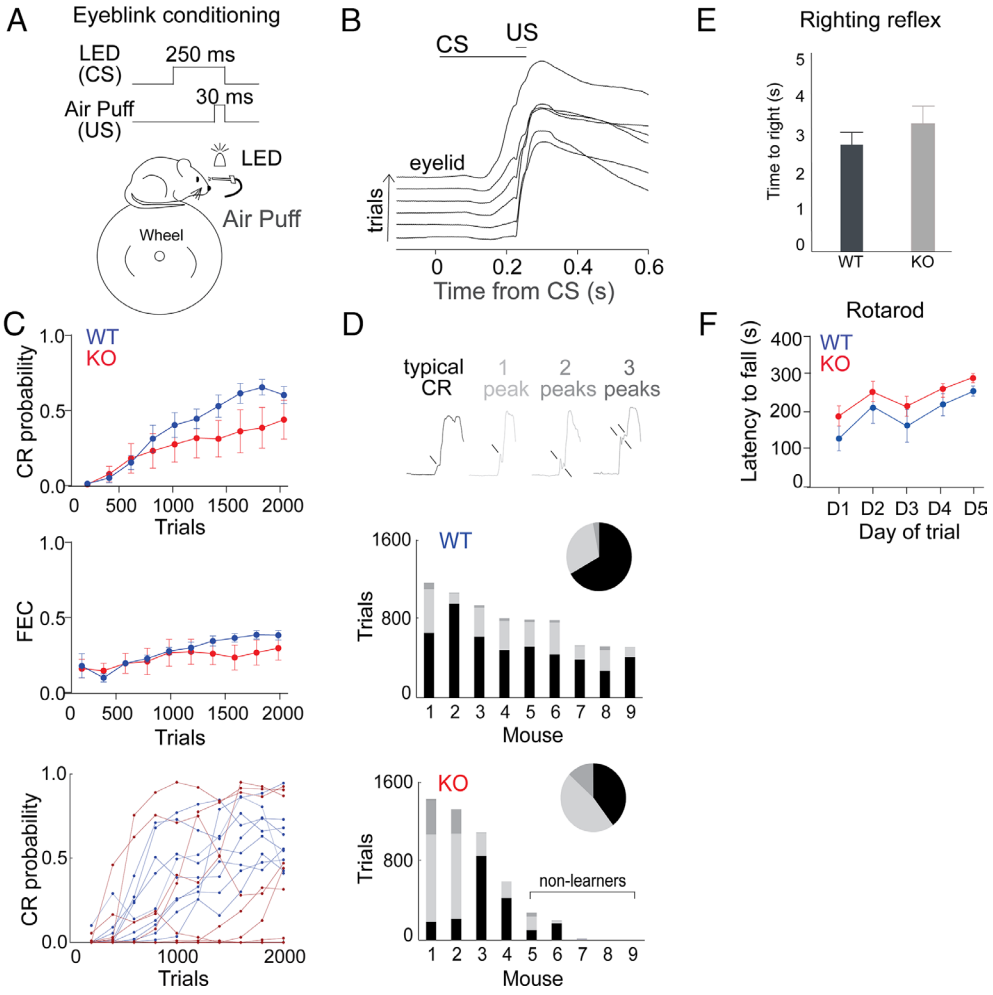

Fig. 3. *Astn2* KO mice show abnormal cerebellar-dependent associative learning but normal righting reflex and rotarod behavior. (*A*) Behavioral configuration for delay eyeblink conditioning. Mice (8 to 15 wk old, N = 9/genotype) were head-fixed and could run freely on a cylindrical treadmill while high-speed videography recorded eyelid position during stimuli presentation. (*B*) Selected average eyelid traces (100-trial average) over the course of training from an example WT mouse in response to a 250-ms LED CS coterminating with the delivery of a 30-ms aversive air puff US. (*C*, *Top*) binned (200-trial average) CR probability over training (last 600 trials $P = 0.14$.) (*Middle*) binned (200-trial average) CR amplitude fraction of eyelid closed (FEC) over training with CRs preserved in trial space (last 600 trials $P = 0.22$). (*Bottom*) CR probability plotted for individual WT (blue) and KO (maroon) mice. (*D*, *Top*) example eyelid traces showing various CR topographies observed during CS-US trials. CRs with three peaks comprised <1% of all observed CRs. (*Middle*) detected CR peaks from all CS-US trials of all WT mice (*Inset*, N = 7,128 trials) and proportional contribution of individual WT mice. (*Bottom*) same as *Middle,* for all CS-US trials of all KO mice (*Inset*, N = 4,943 trials) and proportional contribution of individual KO mice ($P = 0.10$). Data are analyzed with two-tailed unpaired Student's *t* test and presented as mean ± SEM. *E*) P7 WT (n = 12) and Astn2 KO (n = 13) pups were evaluated using the righting reflex assay by placing pups in a supine position. Time to completely right themselves was recorded. No difference was found between WT and KO animals ($P = 0.87$). (*F*) Eight- to twelve-week-old WT (n = 8) and *Astn2* KO (n = 10) animals were placed on an accelerating rotarod for five consecutive days (d). An average of three trials per day was recorded. Time to fall from the rotarod was measured. *Astn2* KO animals had significantly higher latency to fall compared to WT animals [$F(1,80) = 7.0205$, $P = 0.01$]. Data are analyzed with the repeated measures ANOVA test and presented as the mean ± SEM.

eyeblink conditioning, frequently resulting in eyelid closures that have altered kinematics (26).

***Astn2* KO Animals Show Normal Righting Reflex and an Improved Performance on the Rotarod.** As mutations in cerebellar genes often result in motor abnormalities in mice, we investigated motor behavior by testing pup righting reflex and adult mice performance on the accelerating rotarod test. P7 pups were placed on their backs in a supine position. The time taken for the mice to right themselves was measured. *Astn2* KO pups did not significantly differ compared to control mice in the time taken to right themselves (Fig. 3*E*). Next, adult 8 to 12-wk-old mice were placed on a rotarod that accelerated from 4 to 40 RPM in 5 min and were tested on five consecutive days with three trials each day. *Astn2* KO animals did not show defects in balance and coordination. In fact, their performance was significantly better compared to WT littermates (Fig. 3*F*). Thus, while *Astn2* KO animals have ASD-like behaviors they do not exhibit righting reflex deficits or deficits in motor coordination and balance on the rotarod.

PC–Specific Deletion of *Astn2* Recapitulates Some ASD-Like Behaviors. The $Astn2^{flox/flox}$ line was crossed with the *Pcp2-Cre* line to generate a PC-specific conditional KO line. We used this line to study the effect of the loss of *Astn2* in PCs on activity, repetitive behaviors, social behavior, and motor behavior on the rotarod. We found that *Astn2* cKO animals recapitulated behavior seen in the global *Astn2* KO mice in the open-field. Specifically, *Astn2* cKO mice were hyperactive and exhibited some repetitive behaviors (*SI Appendix*, Fig. S4 *A–C*). In the three-chamber test, *Astn2* cKO mice did not show differences in sociability or social novelty preference compared to the control littermates (*SI Appendix*, Fig. S4 *D* and *E*). Using the rotarod, we found that *Astn2* cKO mice did not show motor coordination deficiencies. Their performance on the rotarod was significantly better than that of control littermates (*SI Appendix*, Fig. S4*F*). Therefore,

Astn2 cKO mice show hyperactivity and repetitive behaviors, but not altered behavior in the three-chamber test and no defects in performance on the rotarod.

***Astn2* KO Animals Show Regionally Specific Changes in Spine Number and Morphology.** Different regions of the cerebellum have been implicated in coordinating specific behaviors. The hemispheres, especially Crus1, have been shown to direct social behaviors whereas the posterior vermis directs inflexible and repetitive behaviors (13). Behavior is directly correlated with synaptic connectivity in different parts of the brain. To visualize cerebellar molecular layer synapses in detail, we used Golgi-Cox staining to individually label PCs and examine their dendritic spines. We studied the numbers and subtypes of dendritic spines in three areas of the cerebellum to determine whether the loss of *Astn2* affects spines in different regions of the cerebellum differently. We were especially interested in measuring the number of immature, filopodia-like spines. We analyzed the posterior cerebellar lobule IX and crus 1. The anterior cerebellar lobule III served as a control area that has not been implicated in ASD-like behaviors but directs motor and proprioceptive functions (9). We found no differences in spine numbers or morphology in the anterior cerebellum between WT and *Astn2* KO littermates (Fig. 4*C* and *SI Appendix*, Table S5). In contrast, the posterior cerebellum showed a significant increase in overall spine numbers (Fig. 4 *D*, *i* and *SI Appendix*, Table S5) and a significant difference in the distributions of spine lengths (Fig. 4 *D*, *ii* and *SI Appendix*, Table S5). A closer look at the spine length distributions revealed a significant decrease in the fraction of long, filopodia-like spines in the *Astn2* KO animals compared to controls (Fig. 4 *D*, *iii* and *iv* and *SI Appendix*, Table S5). Additionally, we note that though there was no statistically significant difference in the total count of filopodia (Fig. 4 *D*, *iv* and *SI Appendix*, Table S5), we did see a sharp decrease in the average fraction of filopodia per segment (Fig. 4 *D*, *iii* and *SI Appendix*, Table S5). Crus 1 showed an intermediate phenotype with no differences in spine numbers (Fig. 4 *E*, *i* and *SI Appendix*, Table S5), but a significant difference in spine length distributions (Fig. 4 *E*, *ii* and *SI Appendix*, Table S5), with a decrease in fraction (Fig. 4 *E*, *iii* and *SI Appendix*, Table S5) and total count (Fig. 4 *E*, *iv* and *SI Appendix*, Table S5) of filopodia-like spines in the *Astn2* KO animals. These data support the hypothesis that subtle changes in synaptic numbers and morphology can lead to pronounced differences in behavior.

***Astn2* KO Animals Have Increased Levels of the Neuron–Glial Adhesion Protein ASTN1.** Since ASTN2 functions in receptor trafficking and degradation (1), we analyzed proteomic changes that result from the loss of *Astn2*. We performed proteomic analysis on cerebellar lysates of eight WT and eight KO mice of both sexes. Results revealed a small number of cerebellar proteins that differed

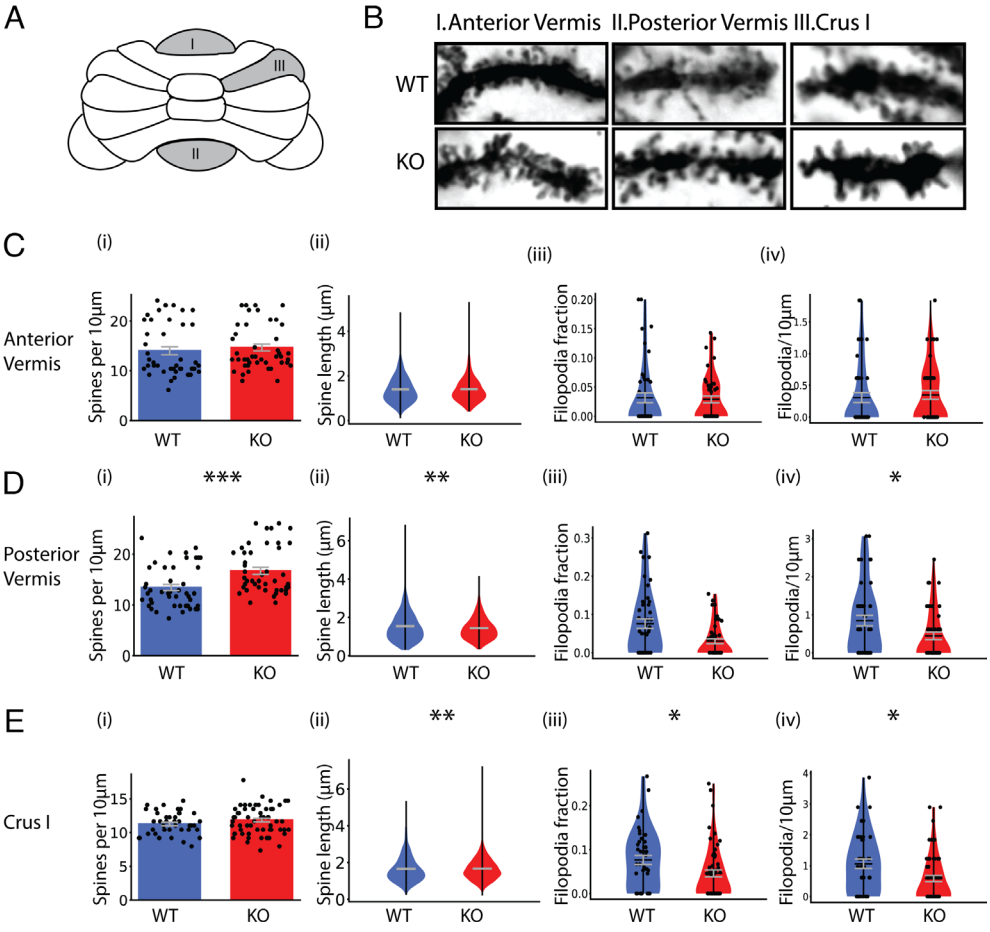

Fig. 4. Cerebellar lobule–specific changes in PC dendritic spine numbers and morphology in *Astn2* KO mice. (*A*) Schematic of a mouse cerebellum. I marks the anterior vermis (lobule III), II marks the posterior vermis (lobule XI), and III marks Crus I. (*B*) Example images of sampled dendritic segments with dendritic spines in the anterior vermis, the posterior vermis, and Crus I, in WT (*Top*) and *Astn2* KO (*Bottom*). (*C*–*E*) Analysis of PC dendritic spines in WT and *Astn2* KO animals in *C* the anterior vermis, (D) the posterior vermis, and (E) Crus I. (*i*) The number of spines per 10 µm dendrite segment (C, $P = 0.1$; D, $P = 0.00016$; E, $P = 0.15$, Wilcoxon rank-sum test.) (*ii*) The distribution of spine lengths with all sampled dendritic segments pooled together (C, $P = 0.078$; D, $P = 0.0038$; E, $P = 0.0047$, two-sample Kolmogorov–Smirnov test.) (*iii*) Distribution of the fractions of filopodia on each sampled dendritic segment. (C, $P = 0.65$; D, $P = 0.064$; E, $P = 0.013$, two-sample Kolmogorov–Smirnov test.) (*iv*) Distribution of the total number of filopodia on each sampled dendritic segment (C, $P = 0.54$; D, $P = 0.029$; E, $P = 0.019$, two-sample Kolmogorov–Smirnov test.)

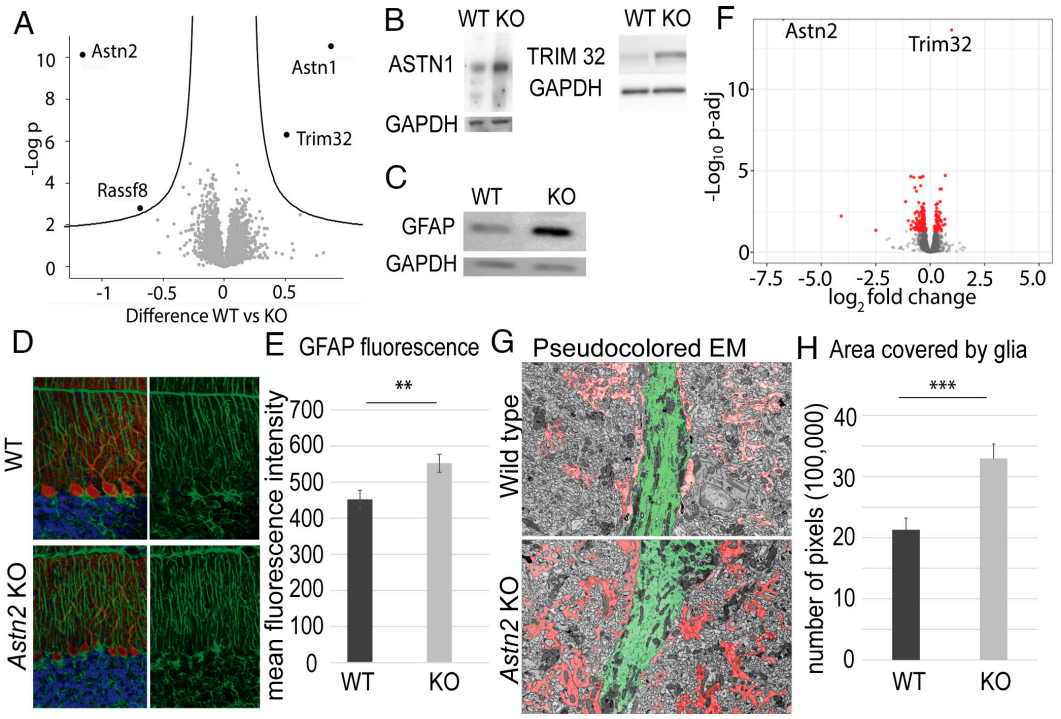

Fig. 5. *Astn2* KO mice have increased levels of ASTN1 and an increase in Bergmann glia. (*A*) Proteomic analysis of *Astn2* KO animals at P22. A volcano plot depicting differentially expressed proteins in whole cerebellar lysates of *Astn2* KO animals and WT littermates (n = 8 WT, 8 KO). ASTN2 is down-regulated and ASTN1 and TRIM32 are up-regulated in *Astn2* KO animals. (*B*) Western blot showing the upregulation of ASTN1 and TRIM32 in P22 cerebellar samples. (*C*) Western blot for GFAP in P22 cerebellar tissue of *Astn2* KO mice. There is an increase in the amount of GFAP protein in *Astn2* KO mice. (*D*) Immunohistochemistry with antibodies against GFAP (a Bergmann glia marker, green), calbindin (a PC marker, red), and Hoechst (blue) in P22 *Astn2* KO mice (*Bottom*) and WT littermates (*Top Left*). An increase in GFAP signal as well as disorganization of BG fibers is observed in *Astn2* KO mice (*Right*). (*E*) *Astn2* KO mice have a higher mean fluorescent intensity of GFAP staining indicating an increase in Bergmann glia ($P = 0.003$). (*F*) Volcano plot depicting differentially expressed genes (P-adj < 0.05, indicated with red) in P22 *Astn2* KO cerebellum, compared with WT littermates, identified using DESeq2. *Astn1* gene is not up-regulated suggesting that ASTN1 protein overexpression is posttranscriptionally regulated in *Astn2* KO animals. (*G*) Electron microscopy imaging of WT (*Top*) *Astn2* KO (*Bottom*) cerebellar molecular layer at P22. An example image of 2,900× direct magnification EM image pseudocolored revealing a PC dendrite (green) and Bergmann glia fibers (red). *H*) Quantification of the area covered by glia in EM images in WT and *Astn2* KO animals. There is a significant increase in Bergmann glia fibers in the *Astn2* KO ($P = 0.0007$). Three mice per genotype for all datasets. Data are presented as the mean + SEM. Data are analyzed with Student's *t* test, *$P < 0.05$, **$P < 0.01$, and ***$P < 0.001$

between genotypes (Fig. 5*A*). ASTN2 protein was highly reduced in the *Astn2* KO, as expected. *Trim32*, a small gene located within an intron of *Astn2* and transcribed from the opposite strand (5), shows a significant increase in protein levels. RASSF8, a protein with no known function in the nervous system, was slightly reduced. Finally, the protein levels of ASTN1, a family member of ASTN2, are increased around twofold in the *Astn2* KO. These results are corroborated by western blotting (Fig. 5*B*). In parallel with proteomic assays, we conducted translating ribosome affinity purification (TRAP) (29, 30) followed by RNA sequencing to examine changes in gene expression after the loss of ASTN2. We crossed *Astn2* KO mice with *Pcp2-Egfp-L10a* mice expressing *EGFP*-tagged ribosomal subunit L10a under the *Pcp2* promoter to specifically profile the PC transcriptome and performed TRAP at P22. As expected, Pcp2 was highly enriched in TRAP samples, whereas the GC marker Neurod1 was enriched in input samples and depleted in TRAP samples (*SI Appendix*, Fig. S5*A*). In line with proteomics, differential analysis revealed only four differentially expressed genes in PCs, including *Astn2* and *Trim32* (*SI Appendix*, Fig. S5*B*). Input samples (whole cerebellum) revealed around 200 differentially expressed genes at a low level (Fig. 5*F*), which did not result in a corresponding change in protein levels. Notably, the expression of *Astn1* mRNA was not changed in *Astn2* KO whole cerebellum or PCs (Fig. 5*F* and *SI Appendix*, Fig. S5 *C* and *D*). These results suggest that increased ASTN1 protein levels likely result from defects in trafficking and degradation caused by the loss of ASTN2 consistent with our previous findings on the trafficking of ASTN1 by ASTN2 (1, 3).

***Astn2* KO Animals Have an Increase in Bergmann Glia (BG).** Previous studies demonstrated that ASTN1 is a neuronal adhesion protein that functions in neuron–glial binding and localizes to adhesion junctions between granule cells and BG during granule cell radial migration in development (2). As BG form contacts with PC spines and are important for PC development and function (31, 32), we tested whether the abundance of ASTN1 protein in the *Astn2* KO might lead to changes in BG morphology or function. We used immunohistochemistry and western blotting to examine the levels of BG marker GFAP in *Astn2* KO and WT littermates at P22. In the *Astn2* KO we observed a significant increase in the antibody signal for GFAP as well as apparent disorganization of BG radial fibers that span the molecular layer (Fig. 5 *D* and *E*) and an increase in protein levels via western blotting (Fig. 5*C*). Next, we used electron microscopy (EM) to perform an ultrastructural analysis of the interactions between BG and PCs in the molecular layer of the cerebellum. By EM, we observed a significant increase, around 50% more, in BG fibers surrounding PCs in *Astn2* KO cerebellum compared to the WT (Fig. 5 *G* and *H*). We did not observe any significant differences in the parallel fiber-PC synaptic ultrastructure between the genotypes in terms of the length of the synapse, the number of vesicles in the synaptic bouton or the contact ratio between the PF terminals and the dendritic spines (*SI Appendix*, Fig. S6). Overall, these data suggest that the increase in BG within the molecular layer of the cerebellum may contribute to the behavioral and molecular defects observed in *Astn2* KO mice.

***Astn2* KOs Show Differences in PCs' Spontaneous and Evoked Synaptic Currents.** Given the changes in spine density and filopodial spines, we next investigated the functional properties of PC synapses in *Astn2* KO animals. Thus, we performed whole-cell electrophysiological recordings in acute brain slices from *Astn2* KO animals (P18–P25) and age-matched WT littermates. Spontaneous EPSCs/IPSCs (sEPSCs/sIPSCs) were recorded to assess the overall level of synaptic input from excitatory parallel fibers (sEPSCs, Fig. 6 *A*, *Top*) and inhibitory basket and stellate cells (sIPSCs, Fig. 6 *B*, *Top*) (Statistical analysis available in *SI Appendix*, Table S6). We observed a decrease in the frequency of sEPSCs (interevent interval, IEI, Fig. 6 *A*, *Bottom Right*) as compared to WTs. We also observed significantly larger sEPSCs in *Astn2* KO animals (Fig. 6 *A*, *Bottom Left*). Inhibitory currents were also altered in *Astn2* KO animals, with significantly larger sIPSCs (Fig. 6 *B*, *Bottom Left*) as compared to WTs. However, we did not observe a difference in sIPSC frequency (Fig. 6 *B*, *Bottom Right*).

We next recorded evoked EPSCs from parallel fibers (Fig. 6 *C*, *Left*) and found that *Astn2* KOs have greater EPSC amplitudes as compared to WTs (Fig. 6 *C*, *Right*). Similarly, we observed a trend toward larger evoked IPSCs (Fig. 6*E*). These results are consistent with our observations of larger sEPSCs and sIPSCs and may reflect an enhanced postsynaptic response. We did not, however, observe any difference in EPSC or IPSC kinetics (Fig. 6 *D* and *F*), suggesting no difference in average synapse location on the somatodendritic axis of PCs, or change in the receptor subunit compositions between WT and *Astn2* KO animals.

Changes in both spontaneous and evoked EPSCs in the *Astn2* KOs could alter the balance of excitation and inhibition, as a bias toward excitation has been linked to cognitive disorders such as ASD (33–35). We therefore also calculated the ratio of excitation to inhibition (E/I ratio, Fig. 6 *G*, *Left*) but found no difference in E/I ratio between *Astn2* KOs and WTs (Fig. 6 *G*, *Right*), consistent with our observation that both spontaneous EPSCs and IPSCs (Fig. 6 *A* and *B*) and evoked EPSCs and IPSCs (Fig. 6 *C* and *E*) increase in tandem with a global KO of *Astn2*.

Supporting the interpretation that changes in synaptic amplitude are due to postsynaptic effects, we found that the paired-pulse ratio of EPSCs onto PCs (PPR, Fig. 6 *H*, *Left*) was unchanged in *Astn2* KO animals (Fig. 6 *H*, *Right*), suggesting no difference in presynaptic release probability. Finally, we measured the intrinsic excitability of PCs using noninvasive cell-attached recordings (Fig. 6 *I*, *Left*) and found no difference in either spiking rate (Hz, Fig. 6 *I*, *Middle*) or coefficient of variation (CV, Fig. 6 *I*, *Right*).

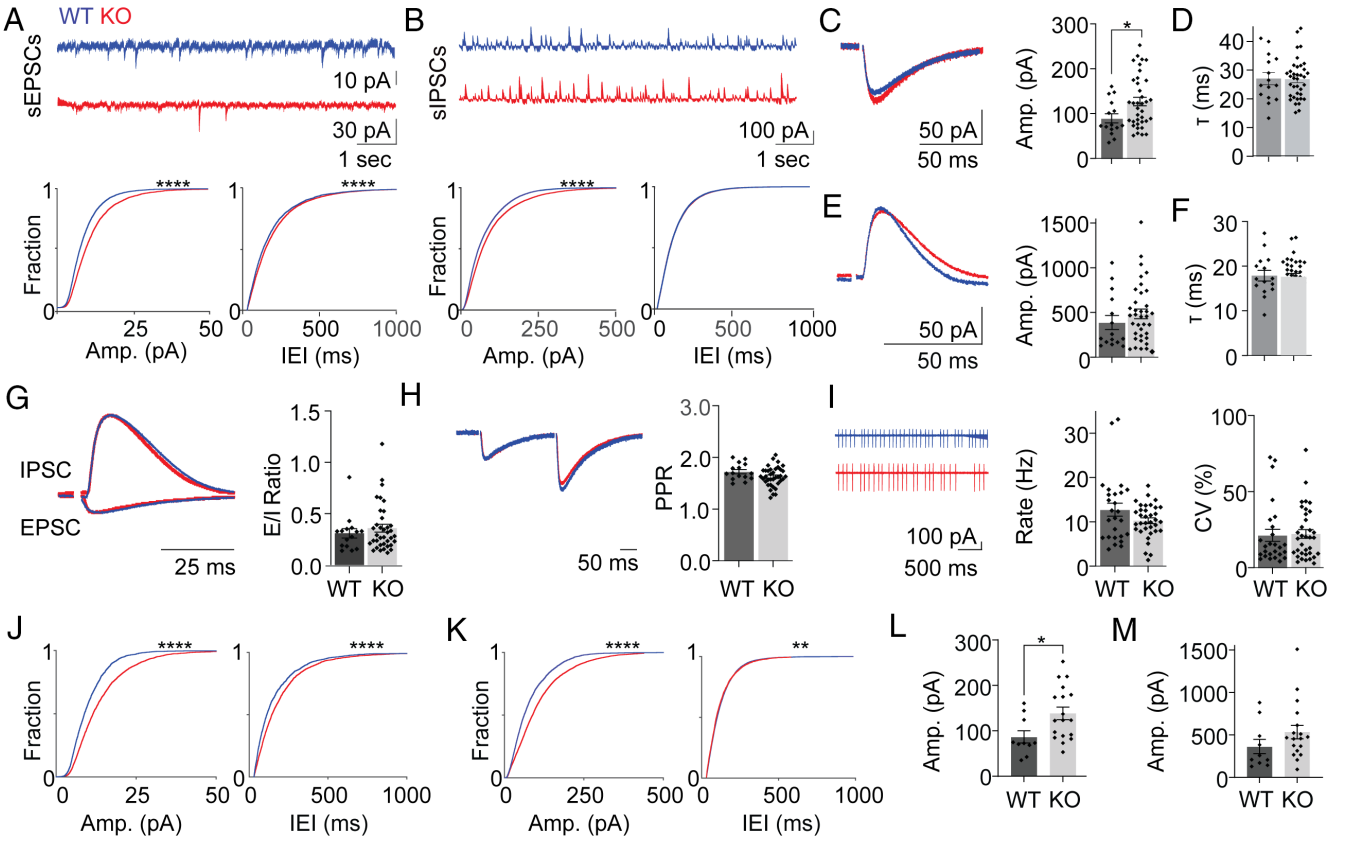

Fig. 6. *Astn2* KO mice show differences in spontaneous and evoked synaptic currents. (*A*, *Top*) sEPSCs in whole-cell recordings (V_m = −70 mV) of PCs. (*Bottom Left*) cumulative distribution of sEPSC amplitudes. *P* = 6.6e-148, Wilcoxon rank-sum test. (*Bottom Right*) same as *Left,* for IEI. *P* = 3.3e-14, Wilcoxon rank-sum test. (*B*, *Top*) sIPSCs in whole-cell recordings of PCs (V_m = 0 mV). (*Bottom Left*) cumulative distribution of sIPSC amplitudes. *P* = 3.5e-123, Wilcoxon rank-sum test. (*Bottom Right*) same as *Left,* for IEI, *P* = 0.99, Wilcoxon rank-sum test. (*C*, *Left*) example of mean evoked EPSC in whole-cell recordings of PCs (V_m = −70 mV). (*Right*) summary of EPSC amplitudes across cells. *P* = 0.02, two-tailed unpaired Student's *t* test. (*D*) Summary of EPSC decay kinetics (τ) across cells. *P* = 0.91, two-tailed Student's *t* test. (*E*, *Left*) example of mean evoked IPSC in whole-cell recordings of PCs (V_m = 0 mV). (*Right*) summary of IPSC amplitudes across cells. *P* = 0.33, two-tailed unpaired Student's *t* test. (*F*) Summary of IPSC τ across cells. *P* = 0.94, two-tailed unpaired Student's *t* test. (*G*, *Left*) example of mean evoked EPSC and IPSC from an individual WT and KO PC. KO traces scaled to the WT EPSC. (*Right*) summary of the ratios of excitation to inhibition (E/I ratio) across cells. *P* = 0.46, two-tailed unpaired Student's *t* test. (*H*, *Left*) example of mean evoked EPSCs from an individual WT and KO PC. KO traces scaled to the first WT EPSC. (*Right*) summary of paired-pulse ratios (PPR) across cells. *P* = 0.09, two-tailed unpaired Student's *t* test. (*I*, *Left*) example of mean extracellular recordings of PC spiking activity from an individual WT and KO PC. *Middle,* summary of spike rates across cells. (*Right*) summary of coefficients of variation (CV) across cells. *P* = 0.10, two-tailed unpaired Student's *t* test. (*J*, *Left*) cumulative distribution of sEPSC amplitudes of PCs in the posterior vermis. *P* = 2.0e-106, Wilcoxon rank-sum. (*Right*) same as (*left*) for IEIs. *P* = 1.2e-17, Wilcoxon rank-sum test. (*K*, *Left*) cumulative distribution of sIPSC amplitudes of PCs in the posterior vermis. *P* < 0.0001, Wilcoxon rank-sum test. (*Right*) same as *Left,* for IEIs. *P* = 0.004, Wilcoxon rank-sum test. (*L*) Summary of EPSC amplitudes across PCs in the posterior vermis. *P* = 0.02, two-tailed unpaired Student's *t* test. (*M*) Summary of IPSC amplitudes across PCs in the posterior vermis. *P* = 0.19, two-tailed unpaired Student's *t* test. Error bars ± SEM.

Notably, our recordings were performed in both the anterior and posterior vermis of the cerebellum. Because anatomical differences were most pronounced in the posterior cerebellum, we next subdivided our recordings to specifically assess synaptic responses in this region. Importantly, changes in synaptic transmission were more pronounced in the posterior vermis, with larger differences in both sEPSC amplitude (Fig. 6 *J*, *Left*) and frequency (Fig. 6 *J*, *Right*), as well as sIPSC amplitude (Fig. 6 *K*, *Left*). In this region, we also measured a small but statistically significant reduction in sIPSC frequency (Fig. 6 *K*, *Right*). PCs in the posterior vermis showed larger evoked EPSC amplitudes (Fig. 6*L*) and trend toward larger evoked IPSC amplitudes (Fig. 6*M*). (Statistical analysis available in *SI Appendix*, Table S7.) Together, these measurements suggest both pre- and postsynaptic changes in synaptic transmission. Specifically, the decrease in sEPSC and sIPSC rate suggests fewer functional excitatory and inhibitory synapses onto KO PCs. While our anatomical measurements indicate greater spine numbers, these results may be related to the reduced fraction of filipodial spines in KO animals, or single parallel fibers impinging on more spines (fewer unique contacts). In contrast, the significantly larger sEPSC and sIPSC amplitudes may suggest a postsynaptic enhancement of synaptic transmission, perhaps reflecting larger numbers of postsynaptic AMPA and GABAA receptors at mature spines in KO animals. Overall, these results show subtle but significant changes in the synaptic strength of PCs, with a stronger effect on sEPSCs, suggesting that cerebellar processing is altered by *Astn2* loss of function.

Discussion

Our studies of mice lacking *Astn2* demonstrate an important role for ASTN2 in ASD-related behaviors including communication via USVs, social behavior, hyperactivity, repetitive behaviors, and in cerebellar circuit properties. In addition, mutant animals appear to have reduced cerebellar learning as measured by eyeblink conditioning. Of these phenotypes, PC–specific cKO mice showed hyperactivity, and repetitive behaviors, showing that cerebellar perturbation is sufficient to cause these phenotypes. Proteomic analyses and ultrastructural studies showing an increase in BG volume surrounding PC spines are consistent with changes in neuron–glial interactions. A change in the number and maturity of spines in the posterior vermis and Crus 1 supports the interpretation that ASTN2 is important for spine formation and dynamics in areas of the cerebellum associated with social and repetitive behaviors. Electrophysiological studies show changes in the *Astn2* KO cerebellum, especially in its posterior aspect, consistent with the results on spine changes in this area. In agreement with other studies (18, 19) our studies support the conclusion that subtle changes in cerebellar anatomy and physiology can lead to significant changes in behavior.

As ASDs are characterized by social impairments, repetitive and inflexible behaviors (19, 36), and in many cases, language deficits (1, 37), we focused on analyzing changes in these behaviors in *Astn2* KO mice. The children with ASTN2 mutations we have reported on previously (1) displayed a range of NDD, including intellectual disability and ASD. Two features in particular stood out in the affected children, namely, learning difficulty and speech and language delay, regardless of other diagnoses. While human language cannot be explored in mice, vocal communication behavior is conserved across taxa (38). Our assays of USV calls in a pup separation assay showed a dramatic (40%) decrease in calls and changes in call structure. These findings represent one of the largest decreases in pup isolation calls in mouse models of ASD and are consistent with prior studies on children with *ASTN2* CNVs (1) as well as other studies in mouse models (21, 39). The shorter duration of calls with an unmatched increase in pause duration and a comparable peak amplitude of the sound pressure level, or volume, of the calls that we observed suggest that the reduction in KOs is not due to respiratory difficulties in holding the call. Spectrally, the comparable average pitch frequency of the calls indicates that abnormalities in the laryngeal musculature are likely not driving the call reduction, as the KO mice could reach a similar pitch. The narrowed pitch range and reduced fraction of dynamic calls suggest a less comprehensive composition of syllables among the KO calls compared to those from control littermates. Thus, our analysis reveals early social communicative challenges with the disruption of *Astn2*. As the *Pcp2-Cre* line we used to generate a cKO specific to cerebellar PCs is not expressed until the end of the first postnatal week, we were unable to assay USV call frequency and structure in pups with a PC-specific loss of *Astn2.*

Our findings show that *Astn2* KO animals have impaired social behavior, as measured in the three-chamber tests for sociability and social novelty preference. *Astn2* KO mice exhibited relatively normal sociability as they showed a preference for the social versus a nonsocial stimulus. Nevertheless, they spent less absolute time overall with the social stimulus compared to the control animals. Importantly, *Astn2* KO mice showed no preference for social novelty as they spent the same amount of time with a familiar mouse as with the novel mouse in contrast to controls. This suggests that ASTN2 is important for influencing social behavior. Interestingly, PC-specific *Astn2* cKO animals did not show impairments in social behavior in the three-chamber paradigm, suggesting that other cell types or brain regions contribute more. Recently, a study has reported differences in the spine number, layer thickness, and number of neuronal cell bodies in the hippocampus and prefrontal cortex in *Astn2* KO animals, which may partially explain the differences observed in social behavior (40). More research is needed to elucidate which brain regions contribute to deficits in social behavior in *Astn2* KO animals and the exact contribution of the cerebellum to social behavior, language, and communication.

Astn2 KO animals have a significant increase in hyperactivity and repetitive behaviors as seen in the open-field assay. Repetitive behaviors are a hallmark of ASD, and hyperactivity is a very common comorbidity. In addition, we found that global *Astn2* KOs have a reduced anxiety phenotype in the open-field. A similar result has been recently reported in *Astn2* KOs using an elevated plus-maze test (40). Importantly, we found that PC-specific cKO mice have a similar phenotype to global KO animals in hyperactivity and repetitive behaviors, suggesting that the cerebellum plays an important role in regulating those behaviors.

The fact that we did not observe changes in social behavior in *Astn2* cKO mice is consistent with our anatomical studies showing no, and less pronounced, differences in Crus 1 of the cerebellum in spine numbers and spine morphology, respectively. In comparison, the posterior vermis, which is associated with repetitive behaviors (13), has significant differences in spine and filopodia numbers that correlate well with repetitive behavioral changes seen in *Astn2* cKO. Interestingly, we observed no defects in *Astn2* KO motor reflexes and coordination. *Astn2* KO mice could right themselves as quickly as controls as pups and performed significantly better on the rotarod as adults. Many animal models focusing on the cerebellum and ASD show motor differences, but some do not (for a comprehensive list see ref. 41). In addition, ASD mouse models can show either inferior or enhanced performance on the rotarod (for a comprehensive list see ref. 42). We hypothesize that the localized differences in spine numbers and morphology and the lack of such differences in the anterior lobule of the cerebellum where many motor behaviors are regulated may partially explain

this phenotype. As anatomical and developmental studies did not reveal any significant changes in neurogenesis, glial-guided migration, or formation of the neuronal layers (*SI Appendix*, Figs. S2 and S3), it is unlikely that the behavioral changes were due to defects in basic steps in cerebellar development but rather subtle differences at the level of the synapse.

The molecular analyses we carried out on the *Astn2* KO cerebellum indicated that the primary change after the loss of *Astn2* was a dramatic increase in the protein levels of the neuron–glial ligand ASTN1. This finding is consistent with our prior studies showing that ASTN2 binds to and promotes the trafficking of ASTN1 (1, 3). Prior studies on ASTN1 demonstrated that it functions in neuron–glial adhesion by binding N-cadherin on BG fibers during granule cell radial migration in development (43). In support of changes in neuron–glial binding in the mutant cerebellum, western blotting and immunohistochemistry showed an increase in GFAP protein levels and EM analysis revealed a large increase in the volume of BG processes around PCs in the molecular layer. BG, PCs, and granule cells form a glutamatergic tripartite synapse in the cerebellar cortex. There is a very intimate relationship between PCs and BG both during development, where they influence each other's growth and maturation (31, 32), as well as in adulthood, where BG has a role in synaptic pruning (44) and plasticity (45). BG ensheath PC dendritic spines, which is important for proper functioning of the synapse (46). This raises the possibility that the loss of *Astn2* leads to changes in the stability or plasticity of dendritic spines in mutant animals. Golgi analyses of dendritic spines indeed demonstrated changes in the number and maturation state of spines in mutant animals as they showed an increase in spine number and a reduction in the fraction of filopodial protrusions, considered an immature state of spine maturation (47). It was of special interest that the spine changes we observed were primarily in the posterior vermis, an area associated with inflexible/repetitive behaviors (13). We hypothesize that the increase in BG area as a direct result of the increase in ASTN1 protein levels leads to the increased spine density and disrupted synapse maturation in *Astn2* KO mice. More research is needed to fully validate this hypothesis.

In line with the observed changes in spine density and maturation, we also found corresponding differences in synaptic transmission in *Astn2* KO animals. Specifically, we observed reduced frequencies of spontaneous excitation and inhibition, and increased amplitudes of both spontaneous and evoked excitation and inhibition. Notably, these effects were preferential to the posterior vermis, where anatomical differences were observed. It is somewhat surprising that we observed decreased rates of spontaneous synaptic currents when anatomical measurements showed an overall increase in spine number. However, one possible explanation could be that the increased number of mature spines is also associated with a redundant sampling of parallel fiber inputs (i.e., fewer unique inputs). In agreement with our measurements, such a configuration would result in both the reduced frequency and increased amplitude of events, as the redundant inputs would boost the amplitude of action potential-evoked EPSCs and IPSCs. Fully resolving this question would require the reconstruction of individual parallel fibers and represents an interesting future direction.

Our loss of function *Astn2* studies are consistent with our prior work showing that ASTN2 regulates synaptic protein receptor trafficking and PC synaptic properties (1). As receptor trafficking is critical for synaptic plasticity and function, these findings are also consistent with prior studies implicating defects in pre- and postsynaptic synaptic proteins (e.g., Neurexins, Neuroligins, Synapsin 1 and 2, PSD-95, Cadherins, and Protocadherins, Shank3) (23, 48, 49) in ASD-like behaviors. Our studies on ASTN2, therefore, support the model that changes in circuit properties contribute to ASD-like behaviors. Importantly, the changes in synaptic transmission we observed were relatively subtle. This may explain the lack of obvious motor deficits in these animals and support the idea that even small changes in cerebellar processing can affect cognitive behaviors. Moreover, the preferential deficits we observed in the posterior cerebellum are in line with the suggested role of this area in ASD-like behaviors, and particularly repetitive behaviors. Therefore, our analyses of *Astn2* KO and cKO mice reveal an important role for ASTN2 in ASD-related behaviors and cerebellar circuit properties.

Materials and Methods

Generation of Astn2 KO Lines. Briefly, C57BL/6J mice (The Jackson Laboratory) were used to create the *Astn2* KO and *Astn2*$^{flox/flox}$ mice using CRISPR-Cas9 technology. Details are available in *SI Appendix, Supplementary Methods*. To generate the PC conditional KO mice, a *Pcp2-Cre* line (Gensat) was crossed with the *Astn2* floxed line.

Immunohistochemistry. Briefly, 100 µm vibratome sections were blocked with 15% normal horse serum (Gibco), 0.3% Triton in PBS overnight and then incubated with primary antibodies overnight at 4 °C, washed in PBS 3× 15 min, and incubated with Alexa Fluor® secondary antibodies overnight at 4 °C. Sections were mounted with ProLong® Gold antifade mounting media and covered with 1.5 thickness Fisherbrand cover glass. The list and concentrations of antibodies are available in *SI Appendix, Supplementary Methods*.

Imaging. Immunohistochemistry images were acquired using an inverted Zeiss LSM 880 NLO laser scanning confocal microscope with a Plan-Apochromat 20×/1.4 NA objective lens and 2× digital zoom. Images were acquired by setting the same gain and offset thresholds for all images per experiment, and over/underexposure of signal was avoided. Images were quantified in FIJI/ImageJ (version 1.53c).

Maternal isolation–induced USVs. Briefly, USVs were recorded at P5–P14 following our previously published methods (50). Details are available in *SI Appendix, Supplementary Methods*.

Behavioral experiments.

Three-chamber social behavior apparatus. Animals were tested between 8 and 12 wk of age. Animals were tested in the three-chamber apparatus as previously described. Details are available in *SI Appendix, Supplementary Methods*.

Open-field locomotion. Animals were tested between 8 and 12 wk of age. Animals were tested in the open-field apparatus as previously described. Ligh/dark box apparatus was used as previously described. Details are available in *SI Appendix, Supplementary Methods*.

Righting reflex. P7 pups were removed from their cage during their awake time and placed in a supine position. The time to completely right themselves was measured with a stopwatch by the experimenter. Pups were returned to the cage immediately.

Rotarod. The rotarod machine used is the ENV-575M by Med Associates Inc in accelerating mode. Details are available in *SI Appendix, Supplementary Methods*.

Delay eyeblink conditioning. Surgical procedures are described in *SI Appendix, Supplementary Methods*. The behavioral setup was constructed according to Heiney et al. (28). Briefly, mice were trained during daily sessions of 200 trials in which a 30-ms air puff (30 PSI) was delivered 3 mm from the mouse's right lateral cornea (US) and paired with a coterminating, 250-ms blue LED (CS) positioned 10 cm in front of the mouse with a minimum intertrial interval of 15 s. Full methods are available in *SI Appendix, Supplementary Methods*.

Proteomics. Full methods are available in *SI Appendix, Supplementary Methods*.

Golgi staining and PC dendritic spine analysis. P22 cerebella were processed for Golgi staining using the FD Rapid GolgiStain™ Kit. During processing, 100 µm sections were cut using Laica vibratome (VT1200S; Leica) and mounted with Permount® mounting medium. Slices were imaged using an upright wide-field brightfield Axioplan 2 microscope fitted with a 40× or 63× objective (Zeiss). A total of 3 to 4 P21–P22 mice were imaged per genotype. For each lobule in our analysis (posterior vermis, anterior vermis, and Crus I), a total of 772 to 1,160 spines per genotype per lobule are included in our analysis. These are sampled

from 4 to 5 PCs per lobule per mouse, with three dendritic segments from each PC. Each dendritic segment is either 10 μm (when using a 63× magnification lens) or 16 μm (when using a 40× magnification lens) in length. These segments are normalized when pooled together for statistical analysis. The length of a spine was measured from the edge of the dendritic shaft until the end of the spine length. Spines longer than 2.773 μm were characterized as filopodia. All analyses on PC dendritic spines are performed using custom scripts in Python.

Electron Microscopy and image analysis. Full details on electron microscopy are available in *SI Appendix, Supplementary Methods*. Twenty images were taken in the molecular layer of Crus I (2,900× magnification) from three mice per genotype and analyzed in Adobe Photoshop. Osmium fixation used enhances the membranes and gives the PC cytoplasm a darker appearance, while BG are whitish pale. Purkinje processes are rich in dark mitochondria and stacks of smooth ER, while BG is not. We used the Magic Wand function in Adobe Photoshop to select the glia in the images and saved the selection. We measured the total area of the selection in pixels. For synaptic quantification, 30 synapses per genotype were analyzed.

Brain slice electrophysiology. See *SI Appendix, Supplementary Methods* for acute brain slice preparation details. Briefly, voltage-clamp recordings were sampled at 50 kHz and bandpass filtered at 1 Hz and 15 kHz. Signals were collected and amplified by a Multiclamp 700B amplifier (Molecular Devices) and digitized using a Digidata 1440A (Molecular Devices). Data were acquired using pClamp 10 (Molecular Devices). A cesium internal solution (pH 7.30) was used for whole-cell recordings. Whole-cell, voltage-clamped recordings were performed with membrane holding potentials of −70 mV to isolate EPSCs and 0 mV to isolate IPSCs. More details are available in *SI Appendix, Supplementary Methods*. Every data point in the summary graphs represents an individual cell recording, with multiple cells from each animal. Electrophysiological analyses were performed using custom scripts in MATLAB (MathWorks).

Resource Availability. Further information and requests for resources and reagents should be directed to and will be fulfilled by the lead contact, Mary E Hatten. All unique/stable reagents generated in this study are available from the lead contact with a completed materials transfer agreement. There are restrictions to the availability of mice used in this study due to the lack of an external centralized repository for its distribution and our need to maintain the stock. We are glad to share mice with a completed materials transfer agreement and reasonable compensation by request or for its processing and shipping.

Data, Materials, and Software Availability. RNA sequencing data have been submitted to GEO under accession number GSE254224 (51). Proteomic datasets were submitted to PRIDE project accession PXD052868 (52). Details on access are provided in the *SI Appendix*.

ACKNOWLEDGMENTS. We are grateful to Dr. Erich Jarvis for providing access to USV testing equipment and to Dr. Nathaniel Heintz for providing access to the three-chamber assay system, open-field testing device, and the rotarod. We thank Dr. Carol A. Mason for comments on the EM experiments. We thank Joe Rodriguez and Eve Govek for helping with sample preparation for EM experiments. The Gensat Project provided the *Pcp2-Cre* line used to generate the cKO animals. We thank Drs. Matt Paul and Tom Carroll from the Bioinformatics Resource Center at Rockefeller University for their support with bioinformatics analysis. We thank the Bioimaging Centre at Rockefeller University for its support with imaging and image analysis. Figures were created using BioRender.com. This work was supported by NIH grant 5R01NS116089 (C.H. and M.E.H.); NIH grants R01NS128054 and R01NS112917 (C.H.); Fellowships from the Sigrid Juselius Foundation and the Leon Levy Foundation (K.M.); grant # UL1 TR000043 from the National Center for Advancing Translational Sciences [NCATS, NIH Clinical and Translational Science Award program (M.H.); and NICHD grant P50HD103525 to IDDRC@WUSTL (S.E.M.)].

Author affiliations: [a]Laboratory of Developmental Neurobiology, The Rockefeller University, New York, NY 10065; [b]Neurobiology Department, Duke University, Durham, NC 27710; [c]Department of Psychiatry and the Intellectual and Developmental Disabilities Research Center, Washington University Medical School, St. Louis, MO 63130; [d]InVitro Cell Research LLC, Englewood, NJ 07631; [e]Helen and Robert Appel Alzheimer's Disease Institute, Feil Family Brain and Mind Research Institute, Weill Cornell Medical College, New York, NY 10021; [f]Electron Microscopy Resource Center, The Rockefeller University, New York, NY 10065; [g]Proteomics Resource Center, The Rockefeller University, New York, NY 10065; and [h]Department of Genetics, Washington University Medical School, St. Louis, MO 63130

Author contributions: M.H., K.F., Z.H., K.M., C.H., and M.E.H. designed research; M.H., K.F., Z.H., K.M., J.Z., H.A.P., and C.H. performed research; S.G., S.E.M., S.H., J.D.D. and C.H. contributed new reagents/analytic tools; M.H., K.F., S.E.M., K.M., J.Z., H.A.P., S.H., C.H., and M.E.H. analyzed data; and M.H., K.F., S.E.M., K.M., J.Z., C.H., and M.E.H. wrote the paper.

1. H. Behesti *et al.*, ASTN2 modulates synaptic strength by trafficking and degradation of surface proteins. *Proc. Natl. Acad. Sci. U.S.A.* **115**, E9717–E9726 (2018), 10.1073/pnas.1809382115.
2. G. Fishell, M. E. Hatten, Astrotactin provides a receptor system for CNS neuronal migration. *Development* **113**, 755–765 (1991).
3. P. M. Wilson, R. H. Fryer, Y. Fang, M. E. Hatten, Astn2, a novel member of the astrotactin gene family, regulates the trafficking of ASTN1 during glial-guided neuronal migration. *J. Neurosci.* **30**, 8529–8540 (2010).
4. J. T. Glessner *et al.*, Autism genome-wide copy number variation reveals ubiquitin and neuronal genes. *Nature* **459**, 569–573 (2009).
5. A. C. Lionel *et al.*, Disruption of the ASTN2/TRIM32 locus at 9q33.1 is a risk factor in males for autism spectrum disorders, ADHD and other neurodevelopmental phenotypes. *Hum. Mol. Genet.* **23**, 2752–2768 (2014).
6. I. Menashe, P. Grange, E. C. Larsen, S. Banerjee-Basu, P. P. Mitra, Co-expression profiling of autism genes in the mouse brain. *PLoS Comput. Biol.* **9**, e1003128 (2013).
7. P. Mariën, R. Borgatti, Language and the cerebellum. *Handb. Clin. Neurol.* **154**, 181–202 (2018).
8. F. Van Overwalle, K. Baetens, P. Mariën, M. Vandekerckhove, Social cognition and the cerebellum: A meta-analysis of over 350 fMRI studies. *Neuroimage* **86**, 554–572 (2014).
9. J. D. Schmahmann, X. Guell, C. J. Stoodley, M. A. Halko, The theory and neuroscience of cerebellar cognition. *Annu. Rev. Neurosci.* **42**, 337–364 (2019).
10. F. Van Overwalle, T. D'aes, P. Mariën, Social cognition and the cerebellum: A meta-analytic connectivity analysis. *Hum. Brain Mapp.* **36**, 5137–5154 (2015).
11. T. D. Rogers *et al.*, Reorganization of circuits underlying cerebellar modulation of prefrontal cortical dopamine in mouse models of autism spectrum disorder. *Cerebellum* **12**, 547–556 (2013).
12. I. Carta, C. H. Chen, A. L. Schott, S. Dorizan, K. Khodakhah, Cerebellar modulation of the reward circuitry and social behavior. *Science* **363**, eaav0581 (2019).
13. E. Kelly *et al.*, Regulation of autism-relevant behaviors by cerebellar–prefrontal cortical circuits. *Nat. Neurosci.* **23**, 1102–1110 (2020).
14. S. H. Fatemi *et al.*, Consensus paper: Pathological role of the cerebellum in Autism. *The Cerebellum* **11**, 777–807 (2012).
15. C. Limperopoulos *et al.*, Does cerebellar injury in premature infants contribute to the high prevalence of long-term cognitive, learning, and behavioral disability in survivors? *Pediatrics* **120**, 584–593 (2007).
16. A. D. Kloth *et al.*, Cerebellar associative sensory learning defects in five mouse autism models. *Elife* **4**, e06085 (2015).
17. C. J. Stoodley *et al.*, Altered cerebellar connectivity in autism and cerebellar-mediated rescue of autism-related behaviors in mice. *Nat. Neurosci.* **20**, 1744–1751 (2017).
18. P. T. Tsai *et al.*, Autistic-like behaviour and cerebellar dysfunction in Purkinje cell Tsc1 mutant mice. *Nature* **488**, 647–651 (2012).
19. P. T. Tsai *et al.*, Sensitive periods for cerebellar-mediated autistic-like behaviors. *Cell Rep.* **25**, 357–367 (2018).
20. T. Hirota, B. H. King, Autism spectrum disorder: A Review. *JAMA* **329**, 157–168 (2023).
21. E. Ey *et al.*, The Autism ProSAP1/Shank2 mouse model displays quantitative and structural abnormalities in ultrasonic vocalisations. *Behav. Brain Res.* **256**, 677–689 (2013).
22. N. M. Beard *et al.*, Ultrasound-guided injection through the rotator cuff interval: A clinical perspective of one institution's results and description of technique. *J. Osteopathic Med.* **123**, 571–576 (2023).
23. M. J. Schmeisser *et al.*, Autistic-like behaviours and hyperactivity in mice lacking ProSAP1/Shank2. *Nature* **486**, 56–60 (2012).
24. J. Oristaglio *et al.*, Children with autism spectrum disorders show abnormal conditioned response timing on delay, but not trace, eyeblink conditioning. *Neuroscience* 248, 708–718 (2013).
25. B. C. Reeb-Sutherland, N. A. Fox, Eyeblink conditioning: A non-invasive biomarker for neurodevelopmental disorders. *J. Autism. Dev. Disord.* **45**, 376–394 (2015).
26. J. P. Welsh, J. T. Oristaglio, Autism and classical eyeblink conditioning: Performance changes of the conditioned response related to autism spectrum disorder diagnosis. *Front. Psychiatry* **7**, 137 (2016).
27. D. H. Simmons, H. K. Titley, C. Hansel, P. Mason, Behavioral tests for mouse models of autism: An argument for the inclusion of cerebellum-controlled motor behaviors. *Neuroscience* **462**, 303–319 (2021).
28. S. A. Heiney, M. P. Wohl, S. N. Chettih, L. I. Ruffolo, J. F. Medina, Cerebellar-dependent expression of motor learning during eyeblink conditioning in head-fixed mice. *J. Neurosci.* **34**, 14845–14853 (2014).
29. J. P. Doyle *et al.*, Application of a translational profiling approach for the comparative analysis of CNS cell types. *Cell* **135**, 749–762 (2008).
30. M. Heiman *et al.*, A translational profiling approach for the molecular characterization of CNS cell types. *Cell* **135**, 738–748 (2008).
31. K. Yamada *et al.*, Dynamic transformation of Bergmann glial fibers proceeds in correlation with dendritic outgrowth and synapse formation of cerebellar Purkinje cells. *J. Comp. Neurol.* **418**, 106–120 (2000).
32. K. Yamada, M. Watanabe, Cytodifferentiation of Bergmann glia and its relationship with Purkinje cells. *Anat. Sci. Int.* **77**, 94–108 (2002).
33. V. S. Sohal, J. L. R. Rubenstein, Excitation-inhibition balance as a framework for investigating mechanisms in neuropsychiatric disorders. *Mol. Psychiatry* **24**, 1248–1257 (2019).
34. E. Lee, J. Lee, E. Kim, Excitation/inhibition imbalance in animal models of autism spectrum disorders. *Biol. Psychiatry* **81**, 838–847 (2017).
35. R. Tatti, M. S. Haley, O. K. Swanson, T. Tselha, A. Maffei, Neurophysiology and regulation of the balance between excitation and inhibition in neocortical circuits. *Biol. Psychiatry* **81**, 821–831 (2017).

36. S. S. H. Wang, A. D. Kloth, A. Badura, The cerebellum, sensitive periods, and autism. *Neuron* **83**, 518–532 (2014).
37. M. Pagani *et al.*, Deletion of autism risk gene Shank3 disrupts prefrontal connectivity. *J. Neurosci.* **39**, 5299–5310 (2019).
38. G. Ehret, Development of sound communication in mammals. *Adv. Study Behav.* **11**, 179–218 (1980).
39. A. P. Belagodu, A. M. Johnson, R. Galvez, Characterization of ultrasonic vocalizations of Fragile X mice. *Behav. Brain Res.* **310**, 76–83 (2016).
40. T. Ito *et al.*, Astrotactin 2 (ASTN2) regulates emotional and cognitive functions by affecting neuronal morphogenesis and monoaminergic systems. *J. Neurochem.* **165**, 211–229 (2023).
41. L. Mapelli, T. Soda, E. D'Angelo, F. Prestori, The cerebellar involvement in autism spectrum disorders: From the social brain to mouse models. *Int. J. Mol. Sci.* **23**, 3894 (2022).
42. K. R. Cording, H. S. Bateup, Altered motor learning and coordination in mouse models of autism spectrum disorder. *Front. Cell Neurosci.* **17**, 1270489 (2023).
43. Z. Horn, H. Behesti, M. E. Hatten, N-cadherin provides a cis and trans ligand for astrotactin that functions in glial-guided neuronal migration. *Proc. Natl. Acad. Sci. U.S.A.* **115**, 10556–10563 (2018).
44. Y. M. Morizawa *et al.*, Synaptic pruning through glial synapse engulfment upon motor learning. *Nat. Neurosci.* **25**, 1458–1469 (2022).
45. A. A. Chrobak, Z. Soltys, Bergmann Glia, Long-term depression, and autism spectrum disorder. *Mol. Neurobiol.* **54**, 1156–1166 (2017).
46. J. J. Lippman, T. Lordkipanidze, M. E. Buell, S. O. Yoon, A. Dunaevsky, Morphogenesis and regulation of Bergmann glial processes during Purkinje cell dendritic spine ensheathment and synaptogenesis. *Glia* **56**, 1463–1477 (2008).
47. D. A. Velázquez-Zamora, M. Martínez-Degollado, I. González-Burgos, Morphological development of dendritic spines on rat cerebellar Purkinje cells. *Int. J. Dev. Neurosci.* **29**, 515–520 (2011).
48. D. Reim *et al.*, Proteomic analysis of post-synaptic density fractions from Shank3 mutant mice reveals brain region specific changes relevant to autism spectrum disorder. *Front. Mol. Neurosci.* **10**, 26 (2017).
49. E. Masini *et al.*, An overview of the main genetic, epigenetic and environmental factors involved in autism spectrum disorder focusing on synaptic activity. *Int. J. Mol. Sci.* **21**, 8290 (2020).
50. S. E. Maloney *et al.*, Characterization of early communicative behavior in mouse models of neurofibromatosis type 1. *Autism Res.* **11**, 44–58 (2018).
51. M. Hanzel *et al.*, Mice lacking Astn2 have ASD-like behaviors and altered cerebellar circuit properties, Gene Expression Omnibus. https://www.ncbi.nlm.nih.gov/geo/query/acc.cgi?acc=GSE254224. Deposited 8 March 2024.
52. M. Hanzel *et al.*, Mice lacking Astn2 have ASD-like behaviors and altered cerebellar circuit properties. PRIDE. http://www.ebi.ac.uk/pride/archive/projects/PXD052868. Deposited 5 June 2024.